

Higgs decays to $\gamma l^+ l^-$ in the standard model

Yi Sun^{1*}, Hao-Ran Chang^{2,1†}, Dao-Neng Gao^{1‡}

¹ *Interdisciplinary Center for Theoretical Study, University of Science and Technology of China, Hefei, Anhui 230026 China*

² *Department of Physics and Institute of Solid State Physics, Sichuan Normal University, Chengdu, Sichuan 610066 China*

Abstract

The radiative Higgs decays $h \rightarrow \gamma l^+ l^-$ with $l = e, \mu$ and τ are analyzed in the standard model using $m_h = 125$ GeV. Both tree and one-loop diagrams for the processes are evaluated. In addition to their decay rates and dilepton invariant mass distributions, we focus on the forward-back asymmetries in these modes. Our calculation shows that the forward-backward asymmetries in $h \rightarrow \gamma e^+ e^-$ and $h \rightarrow \gamma \mu^+ \mu^-$ could be up to 10^{-2} while in the $\tau^+ \tau^-$ final state, these asymmetries are below 1%. Thus the forward-backward asymmetries in $h \rightarrow \gamma l^+ l^-$ might be interesting observables in the future precise experiments both to test our understanding of Higgs physics in the standard model and to probe the novel Higgs dynamics in new physics scenarios.

* E-mail: sunyi@mail.ustc.edu.cn

† E-mail: hrchang@mail.ustc.edu.cn

‡ E-mail: gaodn@ustc.edu.cn

1 Introduction

Since the mass term in the gauge theory violates the gauge invariance, the gauge boson in $SU(2) \times U(1)$ is massless. The Higgs mechanism [1] provides a quite simple method to circumvent this constraint. It begins with a gauge invariance theory, which has massless gauge bosons and unstable vacuum, and obtains a theory with massive gauge boson and stable vacuum after the algebraic transformations on the Lagrangian due to the symmetry spontaneous breaking of the vacuum. The simplest form of this mechanism was considered in the standard model (SM) which requires a single neutral boson Higgs. Since all masses of massive particles in the SM are originated from their coupling with Higgs, the Higgs sector plays a key role in our understanding of the nature of the world. Hence the searching for the Higgs boson was one of the most important work in the past few decades and also the main motivation for the construction of the Large Hadron Collider (LHC). After more than forty years searching, we finally found a Higgs-like scalar particle at around 125 GeV recently thanks to the hard work of ATLAS [2] and CMS [3].

The theoretical property of Higgs in the SM has been extensively studied. The analysis of several different decay channels of the new particle shows that its properties are consistent with the elementary Higgs boson in the SM at 1σ confidence level. However, some unexpected signals also appear and the excess events of the diphoton channel has drawn many attentions [4, 5, 6]. Various new physics, such as MSSM [7], Randall Sundrum Radion [8] and so on, claimed they can interpret such enhancement. But due to the limitation of the experiment data now, there is still a long way to distinguish different models.

On the other hand, besides the $h \rightarrow \gamma\gamma$ decay, a complementary channel, the radiative Higgs decays $h \rightarrow \gamma l^+ l^-$ ($l = e, \mu$ and τ) could also provide some useful information on the SM Higgs boson. Actually, these radiative decays have been studied in the literature [9, 10, 11, 12, 13] and the decay rates and invariant mass distributions have been evaluated. In the last two papers [12, 13], the newly reported mass value of the Higgs boson candidate from [2, 3] has been used in the calculations. The main purpose of the present paper is to focus on the angular distributions, in addition to the rates and invariant mass distributions of the decays. It is known that $h \rightarrow \gamma l^+ l^-$ decays receive the different type contributions from both tree and loop diagrams in the SM [9, 10, 12]. The angular distribution, due to the interference of these different contributions to the decay amplitudes, will lead to a quantity, called as the forward-backward (FB) asymmetry, which might be an interesting observable in the future precise experiments to further understand the properties of SM Higgs Boson, as well as to explore new physics in the Higgs sector [14, 15].

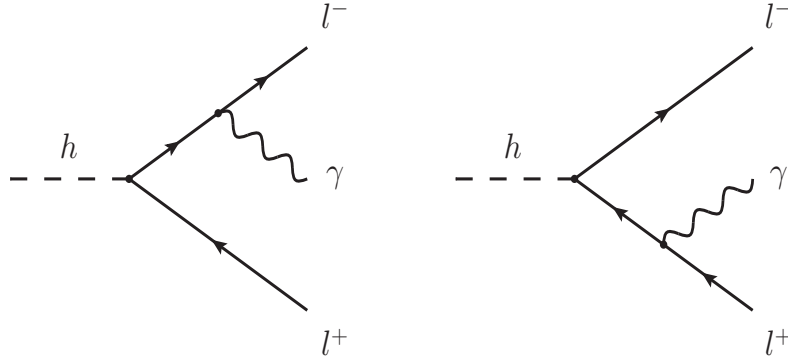


Figure 1: The tree diagrams for $h \rightarrow \gamma l^+ l^-$.

The paper is organized as follows. In section 2, the amplitude of the process $h \rightarrow \gamma l^+ l^-$ from the different diagrams are evaluated, and the expression of the differential decay rate and the FB asymmetries are presented. Section 3 is our numerical analysis and some discussions on phenomenology. Finally, we summarize our conclusions in section 4, and explicit expressions of some loop functions are given in the Appendix.

2 The amplitude of $h \rightarrow \gamma l^+ l^-$

The tree diagrams of the processes $h \rightarrow \gamma l^+ l^-$ are not forbidden, where the photon can be radiated from the lepton leg after Higgs decay to $l^* l$ as shown in Figure 1. Due to the helicity suppression, this contribution is proportional to the mass of lepton. It will be shown that the contribution of the tree diagrams can be neglected safely in the process $h \rightarrow \gamma e^+ e^-$ due to the large mass hierarchy between electron and Higgs, but for $\gamma \mu^+ \mu^-$ and $\gamma \tau^+ \tau^-$ in the final states, the tree diagrams should be included. This is consistent with the results in [9, 10, 12].

Thus from Figure 1, the decay amplitude of $h \rightarrow \gamma l^+ l^-$ at the tree-level can be expressed as follows

$$i\mathcal{M}_t = i\varepsilon_\nu^* C_0 \bar{u}(k_2) \left(\frac{2k_2^\nu + \gamma^\nu \not{p}}{2k_2 \cdot p} - \frac{\not{p} \gamma^\nu + 2k_1^\nu}{2k_1 \cdot p} \right) v(k_1), \quad (1)$$

where $C_0 = -\frac{2\pi\alpha_e m_l}{m_W \sin\theta_W}$, m_l is the mass of lepton, α_e is the fine-structure constant, θ_W is the electroweak mixing angle, and k_1, k_2 and p represent the momentum of l^+, l^- and γ in the final states, respectively.

Since its tree-level amplitude is proportional to the mass of lepton, the next-to-leading contributions could be very important for the $h \rightarrow \gamma l^+ l^-$ transitions, especially for the

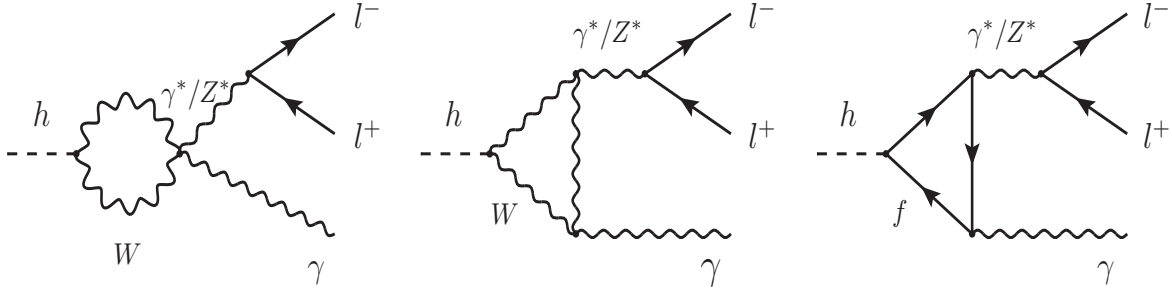


Figure 2: The photon and Z pole one-loop diagrams for $h \rightarrow \gamma l^+ l^-$.

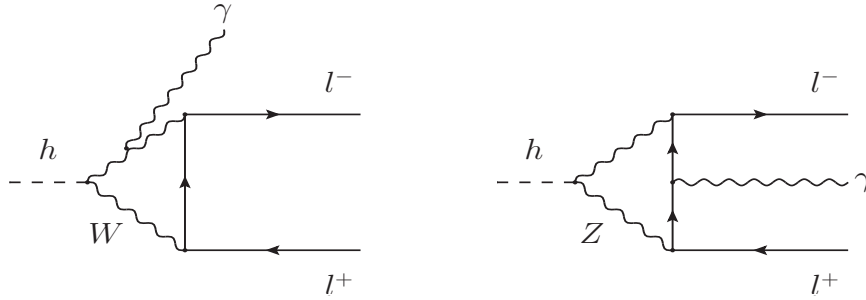


Figure 3: Four-point box diagrams for $h \rightarrow \gamma l^+ l^-$. The photon can also be radiated from another W line in the left diagram and from other charged lepton lines in both diagrams.

electron and muon modes. The typical one-loop Feynman diagrams for these processes have been displayed in Figures 2 and 3, respectively, which are of two basic types: (i) the photon and Z pole diagrams via $h \rightarrow \gamma \gamma^* \rightarrow \gamma l^+ l^-$ and $h \rightarrow \gamma Z^* \rightarrow \gamma l^+ l^-$ (Figure 2); and (ii) four-point box diagrams involving virtual W and Z gauge bosons inside the loop (Figure 3). It has been pointed out by the authors of Ref. [9] that type (i) gives the dominant contributions. Our calculations give the consistent conclusion with [9]. One can check Figures 4, 5, and 6 in the next section for the numerical analysis, that type (ii) diagrams have only very little contributions. In the remainder of this section, for simplicity, we only show explicitly the results from Figure 2, to illustrate the discussions on the differential decay rates and the FB asymmetries. Actually, we include the four-point box diagrams' contributions in our numerical calculations of section 3.

The amplitude of $h \rightarrow \gamma l^+ l^-$ at the one-loop level can be expressed as

$$\begin{aligned}
 i\mathcal{M}_L = & i\varepsilon^{\nu*}[(p_\mu q_\nu - g_{\mu\nu} p \cdot q) \bar{u}(k_2)(C_1 \gamma^\mu + C_2 \gamma^\mu \gamma^5) v(k_1) \\
 & + i\epsilon_{\mu\nu\alpha\beta} p^\alpha q^\beta \bar{u}(k_2)(C_3 \gamma^\mu + C_4 \gamma^\mu \gamma^5) v(k_1)], \tag{2}
 \end{aligned}$$

where

$$\begin{aligned}
C_1 &= -\left(\frac{1}{4} - \sin^2 \theta_W\right) P_Z \Pi_{s\gamma Z} - \frac{1}{q^2} \Pi_{\gamma\gamma}, & C_2 &= \frac{1}{4} P_Z \Pi_{s\gamma Z}, \\
C_3 &= -\left(\frac{1}{4} - \sin^2 \theta_W\right) P_Z \Pi_{a\gamma Z}, & C_4 &= \frac{1}{4} P_Z \Pi_{a\gamma Z}
\end{aligned} \tag{3}$$

with

$$P_Z = \frac{1}{\sin \theta_W \cos \theta_W} \frac{1}{q^2 - m_Z^2 + im_Z \Gamma_Z}. \tag{4}$$

Here we denote q as the momentum of the virtual particle such as γ^* or Z^* in Fig.2, and $q^2 = (k_1 + k_2)^2$ is lepton pair mass squared. $\Pi_{a\gamma Z}$, $\Pi_{s\gamma Z}$ and $\Pi_{\gamma\gamma}$, induced from the Z^* and γ^* pole diagrams in Figure 2, respectively, are given by

$$\Pi_{a\gamma Z} = \frac{\alpha_e^2}{m_W \sin \theta_W} \frac{N_c Q_f T_f}{\sin \theta_W \cos \theta_W} A_{f2}(\tau_f, \lambda_f), \tag{5}$$

$$\begin{aligned}
\Pi_{s\gamma Z} &= \frac{\alpha_e^2}{m_W \sin \theta_W} \left[-\cot \theta_W A_W(\tau_W, \lambda_W) \right. \\
&\quad \left. - 2N_c Q_f \frac{T_f - 2Q_f \sin^2 \theta_W}{\sin \theta_W \cos \theta_W} A_{f1}(\tau_f, \lambda_f) \right],
\end{aligned} \tag{6}$$

$$\Pi_{\gamma\gamma} = \frac{\alpha_e^2}{m_W \sin \theta_W} \left[-A_W(\tau_W, \lambda_W) - 4N_c Q_f^2 A_{f1}(\tau_f, \lambda_f) \right]. \tag{7}$$

Here A_W , A_{f1} , and A_{f2} are functions denoting the contributions from different loops (W loops and fermion loops), with $\tau_i = \frac{4m_i^2}{m_h^2}$, $\lambda_i = \frac{4m_i^2}{q^2}$ ($i = f, W$), and m_f is the mass, N_c is the color multiplicity, Q_f , in unit of e , is the charge, T_f is the third component of weak isospin of the fermion f inside the loop. Expressions for loop functions A_i 's have been shown in the Appendix.

It is easy to see that the γ^* and Z^* pole loop diagrams of Fig. 2 are direct extension of the processes $h \rightarrow \gamma\gamma$ [16] and $h \rightarrow \gamma Z$ [17]. One can recover these results of [16, 17] by setting γ^* and Z^* on-shell in the above expressions excluding the $\Pi_{a\gamma Z}$ parts. The $\Pi_{a\gamma Z}$ part amplitudes, proportional to A_{f2} , receive contributions from the fermion loop diagrams in which Z gauge boson is axial-coupling to the loop fermion. This will generate a parity-odd $h \rightarrow \gamma Z$ amplitude. As is well-known that the $h \rightarrow \gamma Z$ transition is dominated by W -loop contribution, which only leads to the parity-even amplitude. The small parity-odd amplitude is generally neglected in the calculation of $\Gamma(h \rightarrow \gamma Z)$ since it does not interfere with the dominant parity-even amplitude. However, it will be a different story for the $h \rightarrow \gamma l^+ l^-$ decays because the dominant parity-even $h\gamma Z$ vertex can also generate the parity-odd $h \rightarrow \gamma l^+ l^-$ amplitude through the axial-coupling of Z

gauge boson and leptons in the final states. This means that this parity-odd amplitude cannot be simply abandoned in the present work. Such structures have also been shown in Ref. [12]. More interestingly, it will be shown below that, these structures ($\Pi_{a\gamma Z}$ part amplitudes) play a key role in the FB asymmetries of the $h \rightarrow \gamma l^+ l^-$ decays in the SM.

The differential decay rate of $h \rightarrow \gamma l^+ l^-$, including both tree and loop diagrams contributions, can be written as

$$\frac{d\Gamma}{dq^2 d\cos\theta} = \frac{(m_h^2 - q^2)}{512\pi^3 m_h^3} \beta_l [|C_0|^2 A + 2\text{Re}(C_0 C_1^*) B + 2\text{Re}(C_0 C_4^*) C + (|C_1|^2 + |C_3|^2) D + (|C_2|^2 + |C_4|^2) E + 2\text{Re}(C_1 C_4^* + C_2 C_3^*) F] \quad (8)$$

with

$$A = \frac{16}{(m_h^2 - q^2)^2 (1 - \beta_l^2 \cos^2 \theta)^2} [m_h^4 + q^4 + 32m_l^4 - 8m_l^2 q^2 - 8m_l^2 m_h^2 - (m_h^4 + q^4 - 8m_l^2 q^2) \beta_l^2 \cos^2 \theta], \quad (9)$$

$$B = 8m_l \frac{m_h^2 - q^2 + q^2 \beta_l^2 (1 - \cos^2 \theta)}{1 - \beta_l^2 \cos^2 \theta}, \quad (10)$$

$$C = \frac{8m_l (m_h^2 - q^2)}{1 - \beta_l^2 \cos^2 \theta} \beta_l \cos \theta, \quad (11)$$

$$D = \frac{(m_h^2 - q^2)^2}{2} (q^2 + 4m_l^2 + q^2 \beta_l^2 \cos^2 \theta), \quad (12)$$

$$E = \frac{(m_h^2 - q^2)^2}{2} q^2 \beta_l^2 (1 + \cos^2 \theta), \quad (13)$$

$$F = (m_h^2 - q^2)^2 q^2 \beta_l \cos \theta, \quad (14)$$

where $\beta_l = \sqrt{1 - \frac{4m_l^2}{q^2}}$, θ is the angle between the three momentum of Higgs boson and the three momentum of l^- in the dilepton rest frame, and the phase space is given by

$$4m_l^2 \leq q^2 \leq m_h^2, \quad -1 \leq \cos \theta \leq 1.$$

The contribution of the tree diagrams is given by A term in eq. (8) and this term will be divergent when $q^2 \rightarrow m_h^2$, which corresponds to the soft photon in the final states. To avoid such divergence, we cut the minimal energy of photon at 1 GeV when we carry out the integration over q^2 . B and C terms show the interference between the tree and one-loop diagrams and they are both suppressed by the mass of lepton. The last three terms D , E , and F , originate from the contribution of the one-loop diagrams.

Although C and F terms, which are proportional to $\cos \theta$, do not contribute to the decay rate, these two terms will lead to a very interesting observable, called as the FB

asymmetry, which is defined as

$$A_{\text{FB}}(q^2) = \frac{\int_0^1 \frac{d\Gamma}{dq^2 d\cos\theta} d\cos\theta - \int_{-1}^0 \frac{d\Gamma}{dq^2 d\cos\theta} d\cos\theta}{\int_0^1 \frac{d\Gamma}{dq^2 d\cos\theta} d\cos\theta + \int_{-1}^0 \frac{d\Gamma}{dq^2 d\cos\theta} d\cos\theta}, \quad (15)$$

and the corresponding integrated FB asymmetry over q^2 is

$$\mathcal{A}_{\text{FB}} = \frac{\int_{q_{\text{min}}^2}^{q_{\text{max}}^2} \int_0^1 \frac{d\Gamma}{dq^2 d\cos\theta} d\cos\theta dq^2 - \int_{q_{\text{min}}^2}^{q_{\text{max}}^2} \int_{-1}^0 \frac{d\Gamma}{dq^2 d\cos\theta} d\cos\theta dq^2}{\int_{q_{\text{min}}^2}^{q_{\text{max}}^2} \int_0^1 \frac{d\Gamma}{dq^2 d\cos\theta} d\cos\theta dq^2 + \int_{q_{\text{min}}^2}^{q_{\text{max}}^2} \int_{-1}^0 \frac{d\Gamma}{dq^2 d\cos\theta} d\cos\theta dq^2}, \quad (16)$$

where $(q_{\text{min}}^2, q_{\text{max}}^2)$ denotes the range of the integration over q^2 . From eq. (8), one can thus find that the nonzero C_3 or C_4 , which is proportional to $\Pi_{a\gamma Z}$, is required to generate the nonzero FB asymmetries in the SM. Since C term is proportional to m_l , it is expected that F term would give the dominant contributions to the FB asymmetries in $h \rightarrow \gamma e^+ e^-$ and $h \rightarrow \gamma \mu^+ \mu^-$ decays.

We adopt different kinematical variables for the differential decay rate from those in Refs. [12, 13] because we are more concerned about the FB asymmetries in the present work. As we shall see, the $\cos\theta$ dependence in the differential decay rate could provide some interesting information in $h \rightarrow \gamma l^+ l^-$ decays.

3 Numerical analysis

3.1 Decay rates and invariant mass distributions of $h \rightarrow \gamma l^+ l^-$

Both tree and loop diagrams can contribute to the $h \rightarrow \gamma l^+ l^-$ decays, and the amplitudes at the tree-level are proportional to the mass of the lepton in the final states. Our numerical calculation shows that, for $m_h = 125\text{GeV}$ in the SM,

$$\frac{\Gamma(h \rightarrow \gamma e^+ e^-)}{\Gamma(h \rightarrow \gamma\gamma)} = 5.7\% \quad (17)$$

for the electron mode, and the contribution of tree diagrams is vanishingly small; for the muon mode,

$$\frac{\Gamma(h \rightarrow \gamma \mu^+ \mu^-)}{\Gamma(h \rightarrow \gamma\gamma)} = 5.8\%, \quad (18)$$

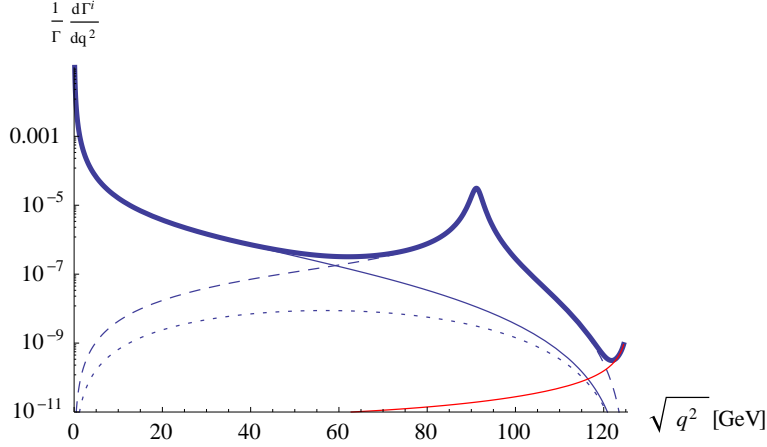


Figure 4: The invariant mass distributions of $h \rightarrow \gamma e^+ e^-$ normalized by $\Gamma(h \rightarrow \gamma\gamma)$. The red line denotes the contribution of the tree diagrams, the thin solid line denotes the contribution from the γ^* pole diagrams, and the dashed line the contribution from the Z^* pole diagrams while the thick line gives the total contributions. The dotted line denotes the contribution from the four-point box diagrams.

and its tree diagram could play a relevant role, which gives about 30% contribution to the rate; while in the process $h \rightarrow \gamma\tau^+\tau^-$, we have

$$\frac{\Gamma(h \rightarrow \gamma\tau^+\tau^-)}{\Gamma(h \rightarrow \gamma\gamma)} = 3.04, \quad (19)$$

where the tree-level contribution is dominant, and the loop diagrams give about 1% contribution. As mentioned above, in order to avoid the infrared divergence from the tree diagrams, we cut the minimal energy of photon at 1 GeV to illustrate our results of (17), (18) and (19).

The dilepton invariant mass distributions of $h \rightarrow \gamma l^+ l^-$, normalized by $\Gamma(h \rightarrow \gamma\gamma)$, have been given in Figures 4, 5, and 6, respectively. Different types of contributions including the tree diagrams, γ^*/Z^* pole diagrams, and four-point box diagrams, are plotted separately for comparison. It is shown that the four-point box diagrams indeed give a negligible contributions for all three modes, and γ^*/Z^* poles (corresponding to the two peaks) give the dominant contributions to the invariant mass distribution in $h \rightarrow \gamma l^+ l^-$ with $l = e, \mu$. From these three plots, one can readily understand our above results of the decay rates, that the tree diagram contribution is vanishingly small in the $e^+ e^-$ case, relevant in the $\mu^+ \mu^-$ case, and dominant in $\tau^+ \tau^-$ channel. Note that these invariant mass distributions in $h \rightarrow \gamma e^+ e^-$ and $h \rightarrow \gamma \mu^+ \mu^-$ have been studied in Ref. [13] and Ref. [12],

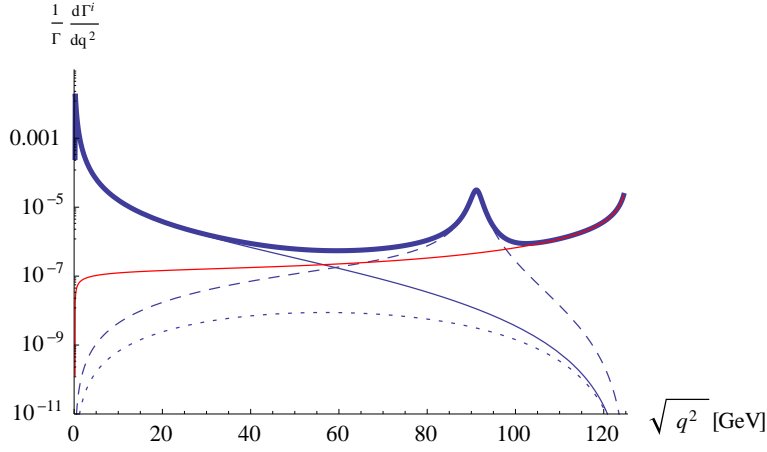


Figure 5: The invariant mass distribution of $h \rightarrow \gamma\mu^+\mu^-$ normalized by $\Gamma(h \rightarrow \gamma\gamma)$. The red line denotes the contribution of the tree diagrams, the thin solid line denotes the contribution from the γ^* pole diagrams, and the dashed line the contribution from the Z^* pole diagrams while the thick line gives the total contributions. The dotted line denotes the contribution from the four-point box diagrams.

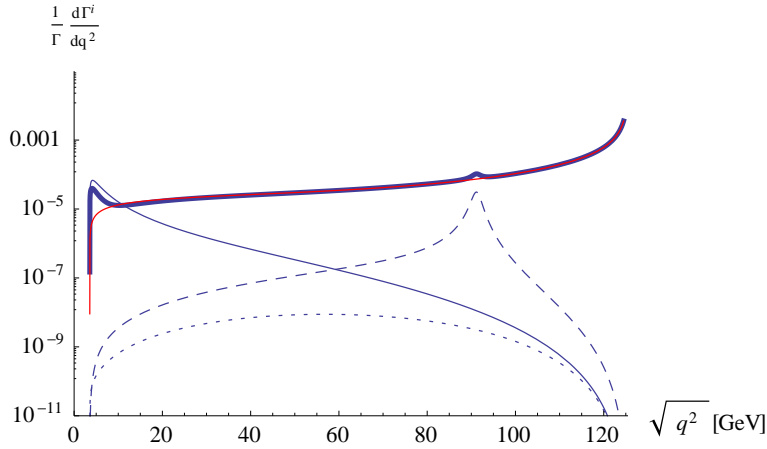


Figure 6: The invariant mass distribution of $h \rightarrow \gamma\tau^+\tau^-$ normalized by $\Gamma(h \rightarrow \gamma\gamma)$. The red line denotes the contribution of the tree diagrams, the thin solid line denotes the contribution from the γ^* pole diagrams, and the dashed line the contribution from the Z^* pole diagrams while the thick line gives the total contributions. The dotted line denotes the contribution from the four-point box diagrams.

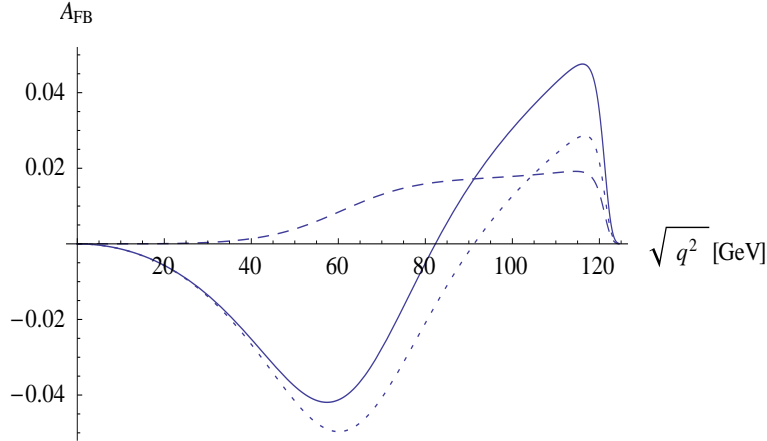


Figure 7: The FB asymmetry $A_{\text{FB}}(q^2)$ in $h \rightarrow \gamma e^+ e^-$ as a function of q^2 . The dotted line denotes the contribution from the γ^*-Z^* interference, and the dashed line denotes the contribution from the Z^*-Z^* interference while the solid line gives the total contribution. The contribution through the interference between the tree diagram and Z^* pole diagrams is extremely small to be shown here.

respectively. One can find that our plots (Figures 6 and 7) are basically consistent with those results. However, because of the different cuts and different normalization, it is not easy to perform a detailed comparison.

3.2 Forward-backward asymmetries in $h \rightarrow \gamma l^+ l^-$

As expected in section 2, the FB asymmetries $A_{\text{FB}}(q^2)$ in $h \rightarrow \gamma e^+ e^-$ and $h \rightarrow \gamma \mu^+ \mu^-$ decays mainly arise from the F term in eq. (8), which, by recalling eq. (3), consists of the contributions from the interference between the γ^* pole amplitude and the Z^* pole amplitude (referred as γ^*-Z^* interference), and from the interference among the different amplitudes of Z^* pole diagrams (referred as Z^*-Z^* interference); while C term contribution generated from the interference between tree and loop diagrams could be neglected or very small. This is confirmed by our numerical calculations.

The FB asymmetries $A_{\text{FB}}(q^2)$ in $h \rightarrow \gamma e^+ e^-$ and $h \rightarrow \gamma \mu^+ \mu^-$ have been plotted in Figures 7 and 8, respectively, which, in most kinematical region, could be up to 10^{-2} . One can see that the C term contribution is very small for the muon mode, and we even do not plot this part contribution in Figure 7 since it is extremely small to be shown. Figure 9 gives the FB asymmetry in $h \rightarrow \gamma \tau^+ \tau^-$, which is about one order of magnitude smaller than the former two modes. It is thought that C term contribution in eq. (8) might be

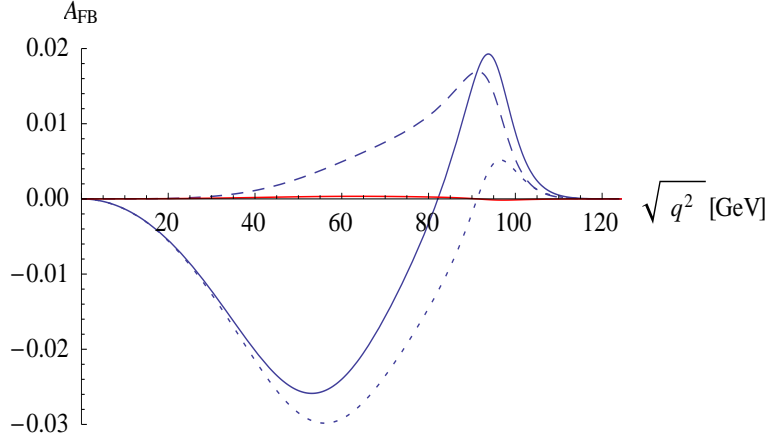


Figure 8: The FB asymmetry $A_{\text{FB}}(q^2)$ in $h \rightarrow \gamma\mu^+\mu^-$ as a function of q^2 . The dotted line denotes the contribution from the γ^* - Z^* interference, and the dashed line denotes the contribution from the Z^* - Z^* interference, and the red line denotes the very small contribution through the interference between the tree diagram and Z^* pole diagrams while the solid line gives the total contribution.

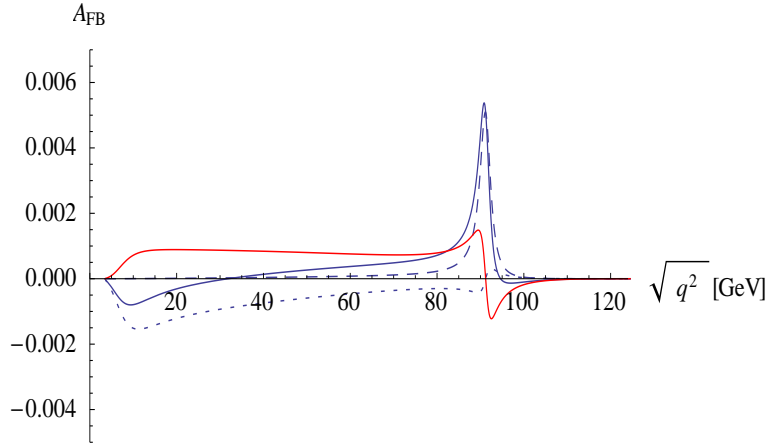


Figure 9: The FB asymmetry $A_{\text{FB}}(q^2)$ in $h \rightarrow \gamma\tau^+\tau^-$ as a function of q^2 . The dotted line denotes the contribution from the γ^* - Z^* interference, the dashed line denotes the contribution from the Z^* - Z^* interference, and the red line denotes the contribution through the interference between the tree diagram and Z^* pole diagrams while the solid line gives the total contribution.

$q_{\min}^2 - q_{\max}^2 (\text{GeV}^2)$	10 ² -30 ²	30 ² -50 ²	50 ² -70 ²	70 ² -90 ²	90 ² -110 ²	full phase space
$h \rightarrow \gamma e^+ e^-$	-0.5%	-2.3%	-3.7%	0.8%	1.9%	0.4%
$h \rightarrow \gamma \mu^+ \mu^-$	-0.4%	-1.9%	-2.3%	0.7%	1.5%	0.4%

Table 1: The integrated FB asymmetries \mathcal{A}_{FB} for some cuts on q^2 in $h \rightarrow \gamma e^+ e^-$ and $h \rightarrow \gamma \mu^+ \mu^-$ decays.

important for τ channel, however, the tree-level amplitude is strongly dominant over the other amplitudes, which, from eq. (15), obviously leads to the suppression of $A_{\text{FB}}(q^2)$ in $h \rightarrow \gamma \tau^+ \tau^-$.

As shown in Figures 7 and 8, $A_{\text{FB}}(q^2)$ in $h \rightarrow \gamma e^+ e^-$ and $h \rightarrow \gamma \mu^+ \mu^-$ will be from negative to positive when q^2 is running in the phase space. This comes from that the $\gamma^* - Z^*$ interference will change sign for q^2 crossing m_Z^2 , since, in this case, the real part of P_Z in eq. (4) changes sign. Thus the integrated FB asymmetries \mathcal{A}_{FB} defined in eq. (16) may be not very significant if we integrate q^2 in the full phase space. On the other hand, when we calculate these integrated asymmetries for some cuts on q^2 , \mathcal{A}_{FB} could be at percent level. The corresponding numerical results have been given in Table 1, and \mathcal{A}_{FB} in the full phase space of q^2 is only 0.4% for both modes. While for some kinematical regions, these asymmetries might be enhanced, for instance, $50 \text{ GeV} < \sqrt{q^2} < 70 \text{ GeV}$, the magnitude of \mathcal{A}_{FB} is 3.7% for $h \rightarrow \gamma e^+ e^-$ and is 2.3% for $h \rightarrow \gamma \mu^+ \mu^-$. In the process $h \rightarrow \gamma \tau^+ \tau^-$, the integrated FB asymmetry will be also very small, $\mathcal{A}_{\text{FB}} \sim 0.02\%$ in the full phase space of q^2 . Therefore it is not significant to calculate them for any cuts on q^2 .

4 Summary and Conclusions

We have presented a comprehensive analysis of the radiative Higgs decays $h \rightarrow \gamma l^+ l^-$ with $l = e, \mu$ and τ in the SM, by using $m_h = 125 \text{ GeV}$, the newly reported mass value of the Higgs boson candidate from LHC [2, 3]. Both tree and one-loop Feynman diagrams for the processes are evaluated. It is found that loop amplitudes are dominant for both electron and muon modes. The tree-level contribution can be fully neglected in $h \rightarrow \gamma e^+ e^-$ decay, and for the muon mode, it will give a sizable contribution to the decay rate while the tree-level transition is very important in $h \rightarrow \gamma \tau^+ \tau^-$. Our numerical results show that $\Gamma(h \rightarrow \gamma l^+ l^-)$ with $l = e, \mu$ is about 6% of $\Gamma(h \rightarrow \gamma \gamma)$, and $\Gamma(h \rightarrow \gamma \tau^+ \tau^-)$ is about factor three of the diphoton rate, which is almost entirely contributed by the tree diagrams. The dilepton invariant mass distributions, normalized by $\Gamma(h \rightarrow \gamma \gamma)$, have been analyzed for all three modes. Different types of contributions are plotted separately

for comparison, the four-point box diagrams are found to be negligible, and the photon and Z pole diagrams give the dominant contribution in $h \rightarrow \gamma e^+ e^-$ and $h \rightarrow \gamma \mu^+ \mu^-$. Our results are basically consistent with those of Ref. [12] and Ref. [13], in which the different cuts and normalization have been used.

One of the main motivation of the present work is to investigate the FB asymmetries in $h \rightarrow \gamma l^+ l^-$. Different from the two-body decay $h \rightarrow \gamma\gamma$, three-body radiative decay may generate a nontrivial angular distribution, which would provide some complementary information for the diphoton decay. In the SM, thanks to the parity-odd $h \rightarrow \gamma Z^*$ amplitude induced from the fermion loop, nonzero FB asymmetries can be expected, and we have explicitly evaluated the SM contributions to $A_{\text{FB}}(q^2)$ and \mathcal{A}_{FB} in these decays. Interestingly, these asymmetries can be up to 10^{-2} in $h \rightarrow \gamma e^+ e^-$ and $h \rightarrow \gamma \mu^+ \mu^-$ decays while they are suppressed below 1% for the $\gamma \tau^+ \tau^-$ final states. Consider the magnitude of these asymmetries, the measurement of them is indeed not an easy task; nevertheless, experimental studies of the FB asymmetries in $h \rightarrow \gamma l^+ l^-$ decays in the future would be very helpful both to increase our understanding of the properties of SM Higgs boson and to probe the novel couplings of Higgs in the new physics scenarios.

In summary, our present analysis indicates that the radiative Higgs decays $h \rightarrow \gamma l^+ l^-$ are worth to be seriously considered in the future experimental investigations. These decays, due to their complementarity to the $h \rightarrow \gamma\gamma$ decay, may provide us with some valuable information on the Higgs physics in the SM and its possible extensions.

Acknowledgements

This work was supported in part by the NSF of China under Grant Nos. 11075149 and 11235010, and the 973 project under grant No. 2009CB825200.

Appendix: Loop functions

Here we explicitly show the expressions for some loop functions in section 2.

$$A_{f1}(\tau, \lambda) = I_1(\tau, \lambda) - I_2(\tau, \lambda) , \quad (\text{A.1})$$

$$A_{f2}(\tau, \lambda) = \frac{\tau\lambda}{\lambda - \tau} [2g(\tau) - 2g(\lambda) + f(\tau) - f(\lambda)] , \quad (\text{A.2})$$

$$\begin{aligned} A_W(\tau, \lambda) = & \left[\left(1 + \frac{2}{\tau}\right) \left(\frac{4}{\lambda} - 1\right) - \left(5 + \frac{2}{\tau}\right) \right] I_1(\tau, \lambda) \\ & + 16 \left(1 - \frac{1}{\lambda}\right) I_2(\tau, \lambda) \end{aligned} \quad (\text{A.3})$$

with

$$I_1(\tau, \lambda) = \frac{\tau\lambda}{2(\tau - \lambda)} + \frac{\tau^2\lambda^2}{2(\tau - \lambda)^2}[f(\tau) - f(\lambda)] + \frac{\tau^2\lambda}{(\tau - \lambda)^2}[g(\tau) - g(\lambda)] , \quad (\text{A.4})$$

$$I_2(\tau, \lambda) = -\frac{\tau\lambda}{2(\tau - \lambda)}[f(\tau) - f(\lambda)] , \quad (\text{A.5})$$

where

$$f(\tau) = \begin{cases} \arcsin^2 \frac{1}{\sqrt{\tau}} & \tau \geq 1 \\ -\frac{1}{4} \left[\ln \frac{1+\sqrt{1-\tau}}{1-\sqrt{1-\tau}} - i\pi \right]^2 & \tau < 1 \end{cases} , \quad (\text{A.6})$$

$$g(\tau) = \begin{cases} \sqrt{\tau - 1} \arcsin \frac{1}{\sqrt{\tau}} & \tau \geq 1 \\ \frac{\sqrt{1-\tau}}{2} \left[\ln \frac{1+\sqrt{1-\tau}}{1-\sqrt{1-\tau}} - i\pi \right] & \tau < 1. \end{cases} \quad (\text{A.7})$$

In fact, for $m_h = 125$ GeV, $\tau < 1$ will not be used if we only consider W and top quark loop.

References

- [1] P.W. Higgs, *Broken symmetries, massless particles and gauge fields*, *Phys. Lett.* **12** (1964) 132, *Broken symmetries and the masses of gauge bosons*, *Phys. Rev. Lett.* **13** (1964) 508, *Spontaneous symmetry breakdown without massless bosons*, *Phys. Rev.* **145** (1966) 1156; F. Englert and E. Brout, *Broken symmetries and the masses of vector mesons*, *Phys. Rev. Lett.* **13** (1964) 321; G.S. Guramnik, C.R. Hagen and T.W.B. Kibble, *Global conservation laws and massless particles*, *Phys. Rev. Lett.* **13** (1964) 585; T.W.B. Kibble, *Symmetry breaking in non-Abelian gauge theories*, *Phys. Rev.* **155** (1967) 1554.
- [2] ATLAS Collaboration, G. Aad et al., *Observation of a new particle in the search for the Standard Model Higgs boson with the ATLAS detector at the LHC*, *Phys. Lett.* **B 716** (2012) 1, arXiv:1207.7214[hep-ex].
- [3] CMS Collaboration, S. Chatrchyan et al., *Observation of a new boson at a mass of 125 GeV with the CMS experiment at the LHC*, *Phys. Lett.* **B 716** (2012) 30, arXiv:1207.7235[hep-ex].
- [4] S. Chang, S.K. Kang, J.P. Lee, K.Y. Lee, S.C. Park and J. Song, *Comprehensive study of two Higgs doublet model in light of the new boson with mass around 125 GeV*, arXiv:1210.3439[hep-ph].

- [5] J. Chang, K. Cheung, P. -Y. Tseng and T. -C. Yuan, *Distinguishing Various Models of the 125 GeV Boson in Vector Boson Fusion*, *JHEP* 04 (2012) 058, arXiv:1206.5853[hep-ph].
- [6] P. M. Ferreira, R. Santos, M. Sher and J. P. Silva, *Implications of the LHC two-photon signal for two-Higgs-doublet models*, *Phys. Rev. D* 85 (2012) 077703, arXiv:1112.3277[hep-ph].
- [7] S. Heinemeyer, O. Stal and G. Weiglein, *Interpreting the LHC Higgs Search Results in the MSSM*, *Phys. Lett. B* 710 (2012) 201, arXiv:1112.3026[hep-ph].
- [8] K. Cheung and T.-C. Yuan, *Could the excess seen at 124-126 GeV be due to the Randall-Sundrum Radion?*, *Phys. Rev. Lett.* 108 (2012) 141602, arXiv:1112.4146[hep-ph].
- [9] A. Abbasabadi, D. Browser-Chao, D.A. Dicus and W.W. Repko, *Radiative Higgs boson decays $H \rightarrow f\bar{f}\gamma$* , *Phys. Rev. D* 55 (1997) 5647, hep-ph/9611209.
- [10] A. Abbasabadi and W.W. Repko, *Higgs boson decay to $\mu\bar{\mu}\gamma$* , *Phys. Rev. D* 62 (2000) 054025, hep-ph/0004147.
- [11] Ana Firan and Ryszard Stroynowski, *Internal conversions in Higgs decays to two photons*, *Phys. Rev. D* 76 (2007) 057301, arXiv:0704.3987[hep-ph].
- [12] L.B. Chen, C.F. Qiao and R.L. Zhu, *Reconstructing the 125 GeV SM Higgs boson through $l\bar{l}\gamma$* , arXiv:1211.6058[hep-ph].
- [13] D.A. Dicus and W.W. Repko, *Calculation of the decay $H \rightarrow e\bar{e}\gamma$* , arXiv:1302.2159[hep-ph].
- [14] A.Yu. Korchin and V.A. Kovalchuk, *Polarization effects in the Higgs boson decay to γZ and test of CP and CPT symmetries*, arXiv:1303.0365[hep-ph].
- [15] C.S. Li, S.H. Zhu and C.F. Qiao, *Radiative Higgs boson decays $H \rightarrow f\bar{f}\gamma$ beyond the standard model*, *Phys. Rev. D* 57 (1998) 6928, hep-ph/9801334.
- [16] A.I. Vainshtein, M.B. Voloshin, V.L. Zakharov and M.S. Shifman, *Low-energy theorems for Higgs meson interaction with photons*, *Sov. J. Nucl. Phys.* 30 (1979) 711. L.B. Okua, *Leptons and Quarks* (North-Holland, Amsterdam, 1982).
- [17] L. Bergstrom and G. Hulth, *Induced Higgs couplings to neutral bosons in e^+e^- collisions*, *Nucl. Phys. B* 259 (1985) 137.